Nanoelectronics and Its New Materials – A NEW ERA OF NANOSCIENCE

Nanoelectronics and Its New Materials –
A NEW ERA OF NANOSCIENCE

ZEISS
Seeing beyond

WILEY

Discover the recent advances in electronics research and fundamental nanoscience.

Nanotechnology has become the driving force behind breakthroughs in engineering, materials science, physics, chemistry, and biological sciences. In this compendium, we delve into a wide range of novel applications that highlight recent advances in electronics research and fundamental nanoscience. From surface analysis and defect detection to tailored optical functionality and transparent nanowire electrodes, this eBook covers key topics that will revolutionize the future of electronics.

To get your hands on this valuable resource and unleash the power of nanotechnology, simply download the eBook now. Stay ahead of the curve and embrace the future of electronics with nanoscience as your guide.

ZEISS

Seeing beyond

WILEY

Check for updates

Disulfide-Bridged Dynamic Covalent Triazine Polymer Thin Films by Interface Polymerization: High Refractive Index with Excellent Optical Transparency

Salma Begum,* Ksenia Kutonova, Anna Mauri, Meike Koenig, Ka Chun Chan, Christian Sprau, Christian Dolle, Vanessa Trouillet, Zahid Hassan, Tobias Leonhard, Stefan Heißler, Yolita M. Eggeler, Wolfgang Wenzel, Mariana Kozlowska, and Stefan Bräse*

Exploring innovative strategies for molecular structuring of dynamic materials that combine self-correcting intrinsic reversibility with the robustness of covalent bonds, has been a long-standing objective from applications perspective in fields ranging from molecular engineering to nanotechnology and interfacial science. To establish dynamic covalent chemistry approaches combined with interfacial polymerization, herein, a distinct synthetic approach is reported to develop disulfide-bridged 2D polymeric $C_3N_3S_3$ triazine thin-films by interfacial thiol-disulfide dynamic exchange process crosslinking tritopic planar 1,3,5-triazine-2,4,6-trithiol molecular tectons via intermolecular disulfide formation in the presence of I_2 vapors at the air/water interface under redox condition. The resulting centimeter-scale polymeric thin-films are covalently cross-linked, dynamic in nature, featuring tunable thickness (6–200 nm) and significant morphological variations are realized under the influence of varying reaction time, concentration and types of reducing agents. Notably, $C_3N_3S_3$ polymer thin films exhibit a transflectance of around 99.5% in the range from 430 to 1800 nm, show high refractive indices (1.730–1.488) and optical anisotropy with uniaxial negative birefringence. The $C_3N_3S_3$ free-standing polymer thin-films can be easily transferred to different substrates or possibly into application-relevant forms for device fabrications, making this useful from materials application perspective.

1. Introduction

Molecular structuring of covalently-linked polymeric networks and thin-films have attracted enormous interest due to their diverse applications as separation membranes, sensors, and (opto-)electronics.[1] Engineering covalently-linked polymeric networks with controlled molecular arrangements (2D–3D architecture) and tuning molecular forces and interconnecting bonds that bind molecular tectons together is of fundamental relevance for tailoring the final structural features and functions of the material to a desired application.[2] A variety of covalent linkages including B—O (boronate ester),[3] C—N (imide),[4] C—N (imine),[5] C—N (aromatic system, include triazine, phenazine),[6] and B—N (borazine)[7] covalent bond, have been introduced for interconnecting chemically-programmed diverse building blocks into molecular materials.[8] Dynamic covalent strategies combining intrinsic reversibility with the robustness

S. Begum, K. Kutonova, C. Sprau, Z. Hassan, T. Leonhard, S. Bräse
Material Research Center for Energy Systems (MZE)
Strasse am Forum 7, Bldg. 30.48, 76131 Karlsruhe, Germany
E-mail: salma.begum@kit.edu; braese@kit.edu

A. Mauri, K. C. Chan, W. Wenzel, M. Kozlowska
Institute of Nanotechnology (INT)
Karlsruhe Institute of Technology (KIT)
Hermann-von-Helmholtz-Platz, 76344 Eggenstein-Leopoldshafen,
Germany

The ORCID identification number(s) for the author(s) of this article can be found under https://doi.org/10.1002/adfm.202303929

M. Koenig, S. Heißler
Institute of Functional Interfaces (IFG)
Karlsruhe Institute of Technology (KIT)
Hermann-von Helmholtz-Platz, D-76344 Eggenstein-Leopoldshafen,
Germany

C. Sprau
Institute of Applied Materials
Ceramic Materials and Technologies (IAM-KWT)
Karlsruhe Institute of Technology (KIT)
Haid-und-Neu Str. 7, 76131 Karlsruhe, Germany

C. Dolle, Y. M. Eggeler
Microscopy of Nanoscale Structures & Mechanisms (MNM)
Laboratory for Electron Microscopy (LEM)
Karlsruhe Institute of Technology (KIT)
Engesserstr. 7, 76131 Karlsruhe, Germany

**ADVANCED
SCIENCE NEWS**

www.advancedsciencenews.com

**ADVANCED
FUNCTIONAL
MATERIALS**

www.afm-journal.de

of covalent bonds, where the cross-linking degree can be dynamically controlled, has opened up exciting new horizons of materials exploration.[9] Prominent reversible covalent linkages include thermo-labile alkoxyamine bonds,[10] reversible cycloaddition (e.g., thermoreversible Diels–Alder reactions),[11] thiol-disulfide exchange process,[12] and others have been envisioned for engineering dynamic covalent polymeric materials.[13] The oxidative coupling of thiols (disulfide formation) is well studied, and widely applied in responsive polymer systems (e.g., vesicles for drug delivery),[14] recyclable polymers (thermoplastics and thermosets),[15] and peptide synthesis. However, to the best of our knowledge, so far, disulfide based polymeric thin films by interfacial polymerization methods have been rarely explored.[16] In a recent accomplishment, we introduced the concept of disulfide-mediated polymerization to prepare hyper-crosslinked 3D-homopolymers based on tetrakis-thiophenol monomers via reversible disulfide bond formation.[17] The disulfide-bridged 3D-homopolymer was synthesized in presence of hydrogen peroxide catalyzed by sodium iodide. The reversible nature of the (—S—S—) dynamic covalent linkages owing to their selective sensitivity to reductive environment further enabled postfunctionalization and depolymerization. Exploiting dynamic covalent chemistry, challenges, and opportunities arise depending on the nature of the interconnecting bonds (each has its own merits and demerits) and dimensionality of the system (2D–3D arrangements). Moreover, for further translational potential, addressing stability, processability, morphology preservation, and structural regularity at different lengths that are more critical to functions and certain applications yet to be demonstrated. As polymeric networks are mostly isolated in solid powders and their processability/fabrication, particularly into thin-films and membranes, is challenging, once synthesized have negligible solubility in solvents.[18] In this endeavor, interfacial polymerization methods and development of new dynamic reaction pathways taking place on interfaces are rapidly growing for the fabrication of freestanding high quality films with a long-range order, defined thickness, and tunable properties.[19] In this present work, we now report a distinct approach to disulfide-bridged 2D polymeric triazine thin-films by interfacial thiol-disulfide exchange process crosslinking planar tritopic 1,3,5-triazine-2,4,6-trithiols via intermolecular disulfide cross-linkages formation in the presence of

iodine vapors at the air/water interface containing a reducing agent. The cross-linkable tritopic molecular design and interfacial polymerization technique offers transferable, processable, and flexible polymer 2D thin-films with controllable thicknesses in the range of 6–200 nm as a function of time for 1–24 h at room-temperature and without the need for any stimuli, templates, or preorganization of the monomers. This unanticipated disulfide dynamic chemistry approach and interface-confined polymerization, i.e., the possibility to dynamically modify the reaction equilibrium and simultaneously polymerizing molecular precursors into fine-tuned dynamic polymeric thin-films at the interface, offers certain challenges to overcome and demonstrates advantages compared to the previously reported solution-based conventional synthesis methods that led to insoluble and nonprocessible polymer agglomerates.[20] Due to the intrinsic high refractive index of sulfur ($n \approx 2.0$), the high molar refraction and polarizability and the low molar volumes of aromatic rings, sulfur-based organic polymeric materials exhibit high refractive indices ($n > 1.50$) and excellent transparency in the near infrared (NIR) region of the spectrum which make them particularly intriguing for NIR imaging technologies.[21] $C_3N_3S_3$ triazine thin-films can be transferred to other substrates or possibly into application-relevant forms for device fabrications.

2. Result and Discussion

2.1. Interfacial Synthesis of Disulfide-Bridged Dynamic $C_3N_3S_3$ Triazine Polymer Films
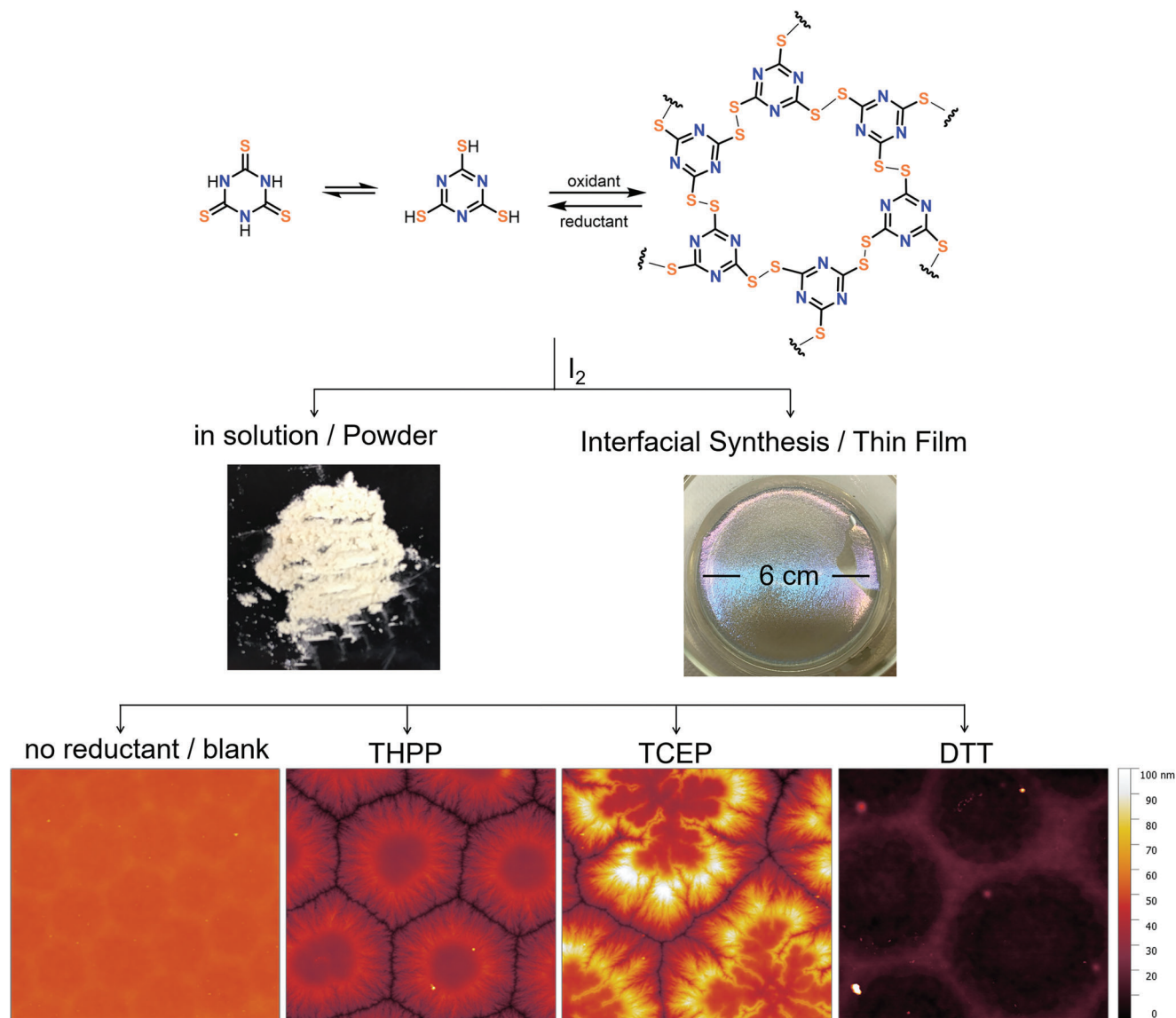
In the current study, tritopic planar tectons of triangular shape bearing predisposed thiol reactive groups at the peripheries (see **Figure 1**) were chosen to generate dynamic covalent polymeric thin-films. 1,3,5-Triazine-2,4,6-trithiol (TTCA) was subjected to thiol oxidation and disulfide reduction conditions simultaneously employing iodine vapors as an oxidizing agent in a closed system at the water interface at room temperature (experimental setup is shown in Figure S1, Supporting Information). Disulfides are generated under oxidative conditions of thiols, while the reducing agent forms thiols from disulfides. In this current study, three different reducing agents, namely tris(hydroxypropyl)phosphine (THPP), tris(2-carboxyethyl)phosphine hydrochloride (TCEP·HCl for simplicity denoted as TCEP) and dithiothreitol (DTT) were investigated. For a reference, blank films were synthesized in the absence of reducing agent under similar experimental conditions. THPP and TCEP are among the extensively used tertiary phosphine-based disulfide reducing agents due to their water-soluble nature and the advantage of being air stable facilitating ease of handling under ambient laboratory conditions. Different concentrations (5, 1, 0.2, and 0.1 eq) of the three reducing agents with respect to TTCA were tested and 0.2 eq was chosen as optimal concentration for the formation of patterned films in all the four cases under similar experimental conditions (see Table S1, Supporting Information). The pH of the four reaction systems were monitored by taking aliquot at 0 min and at time intervals of 4, 6, 10, 14, and 18 h reaction time, gradual decrease in pH was observed as shown in Figure S2 (Supporting Information). Under acidic conditions in the pH range of 3–4, a trend in the patterned film formation was observed in agreement to the reducing

V. Trouillet
Institute of Applied Materials and Karlsruhe Nano
Micro Facility (KNMFi)
Karlsruhe Institute of Technology (KIT)
Hermann-von-Helmholtz-Platz, 76344 Eggenstein-Leopoldshafen,
Germany

K. Kutonova, Z. Hassan, S. Bräse
Institute of Organic Chemistry
Karlsruhe Institute of Technology (KIT)
Fritz-Haber-Weg 6, 76131 Karlsruhe, Germany

T. Leonhard
Light Technology Institute (LTI)
Karlsruhe Institute of Technology (KIT)
Engesserstrasse 13, 76131 Karlsruhe, Germany

S. Bräse
Institute of Biological and Chemical Systems (IBCS-FMS)
Karlsruhe Institute of Technology (KIT)
Hermann-von-Helmholtz-Platz 1, 76344 Eggenstein-Leopoldshafen,
Germany

**ADVANCED
SCIENCE NEWS**

www.advancedsciencenews.com

**ADVANCED
FUNCTIONAL
MATERIALS**

www.afm-journal.de

Figure 1. Interfacial synthesis of disulfide-bridged dynamic covalent $C_3N_3S_3$ triazine polymer thin-films through reversible disulfide bond formation (top); optical images of polymer in powder and film form (middle); AFM topography images showing different surface texture of the films formed in the absence of reducing agent (blank) and by using three different reducing agents THPP, TCEP, and DTT (bottom). All AFM images are 8μm in width. Reduction reaction carried using TTCA monomer (1 eq), respective reducing agent (0.2 eq) in water/THF solvent (9:1 v/v) at room temperature (≈22 °C).

ability of reducing agents (TCEP > THPP > DTT),[22] such as more pronounced hexagonal units are observed in the case of TCEP, THPP, weak in DTT and less pronounced in the case of blank films. On contrary to THPP and TCEP, DTT as a reducing agent is less active in acidic medium (pKa of DTT is ≈8.6),[22] despite this fact the thinnest film (≈50nm) among the three was formed in the presence of DTT. To confirm the active role of reducing agents in the formation of patterned films, we carried the experiments using the oxidized form of TCEP, THPP, and DTT. No patterned films were observed, these results highlight the significance of reducing agents in the formation of patterned films plausibly by regulating the rate of reduction reactions, reaction dynamics and crystallites growth. Other parameters, including reaction time for variable thickness (Figure S2, Supporting In-

formation) and iodine concentration were optimized. Iodine was tested in dissolved form (dissolved in the reaction mixture) and in the form of vapors (self-dissolution in the reaction mixture with time) (Figure S3, Supporting Information).

This protocol exploits the advantages of the dynamic nature of the thiol-disulfide exchange reaction that enables the formation of self-corrected structures due to the labile nature of reversible disulfide bonds with interfacial synthesis that permits attainable rearrangement of building units, nucleation, and growth of extended periodic hexagonal arrays to generate 2D films with tunable thickness. In comparison to the solution-based conventional synthesis methods,[20] synthesis on the water–air interface permits apparently specific preorganization of the TTCA monomers and the regular assemblies direct the formation of ordered,

**ADVANCED
SCIENCE NEWS**

www.advancedsciencenews.com

**ADVANCED
FUNCTIONAL
MATERIALS**

www.afm-journal.de

free-standing $C_3N_3S_3$ triazine polymer thin-films. The 2D polymeric thin-film of $C_3N_3S_3$ features confined molecular arrangements predominantly driven in lateral directions by disulfide covalent linkages and stabilized by noncovalent $\pi-\pi$ stacking. The resultant layered polymer thin films are anticipated to form by strong in-plane disulfide-bridged covalent interactions and weak van der Waals force between the layers. Employing this synthetic approach, centimeter-scale free-standing polymeric thin-films were prepared without advanced/complex instrumentation required. In principle, lateral dimensions of polymeric thin films can be determined by the water surface-size in a vessel available for polymerization.

These films are easily transferable to other substrates, hence allowing convenient structural characterization through various spectroscopic and imaging techniques, and possibly into application-relevant forms for device fabrications.

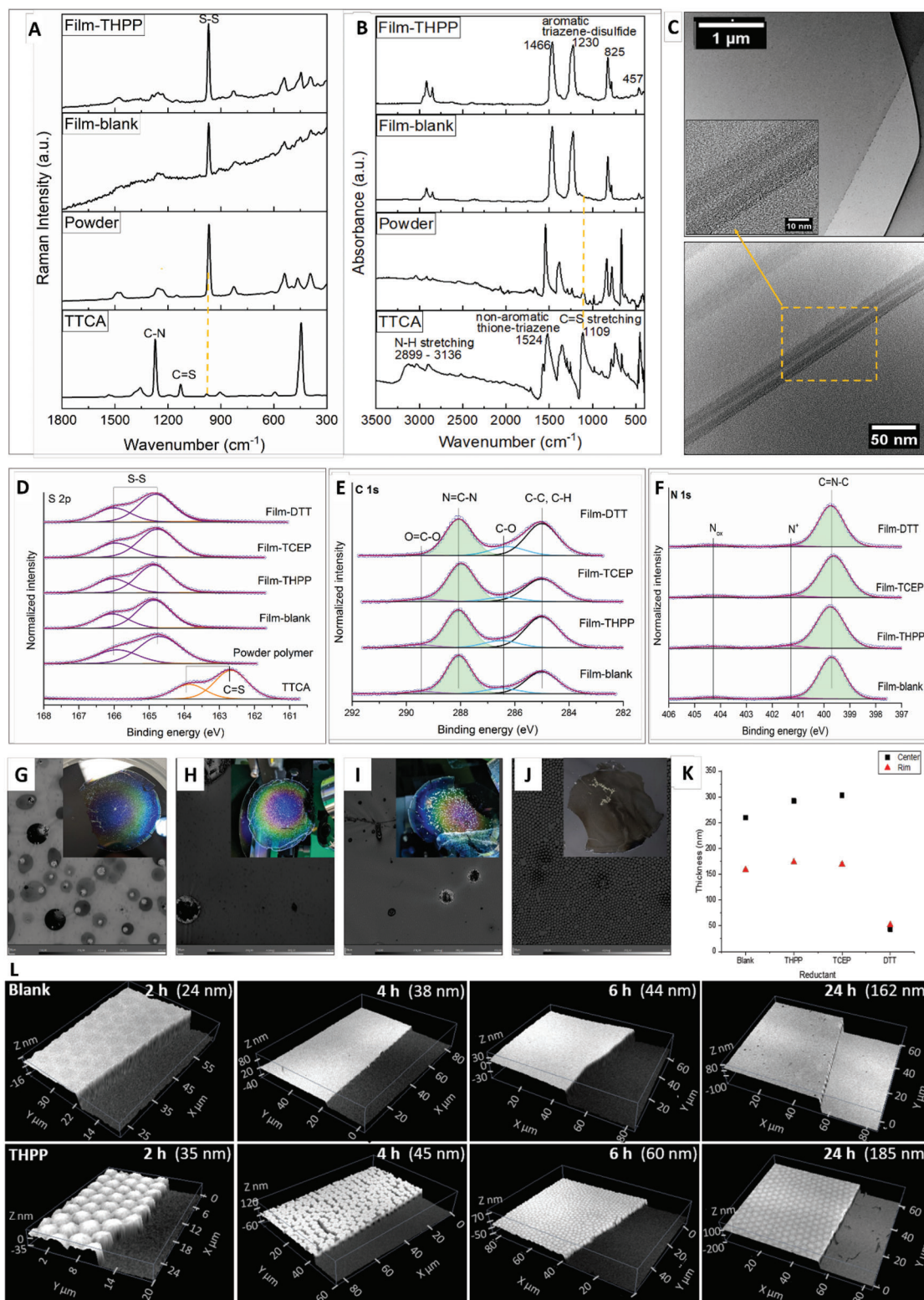## 2.2. Covalent $C_3N_3S_3$ Triazine Polymer Thin-Film Characterization

The molecular structures and morphological patterns of the polymeric films were analyzed by spectroscopic methods and microscopy imaging techniques. Disulfide bond formation in the polymer thin-films was confirmed by Raman and ATR-IR (attenuated total reflection infrared absorption spectroscopy) spectroscopy (**Figure 2**A,B). The formation of disulfide bonds in the polymer thin-films is confirmed by the appearance of an intense band at 966 cm^{-1} assigned to strongly Raman active S—S bending mode, and S—S stretching modes at 498, 512, and 529 cm^{-1}. Vibrational bands at 1125 and 1225 cm^{-1} assigned to the C=S and C—N groups disappear on polymer formation.[23]

The ATR-IR spectra were collected for the monomers TTCA, the polymer in powder form, blank, and THPP films. The TTCA monomers show major bands at 1524, 1109, and 750 cm^{-1} which are characteristics of the nonaromatic, trithione form of triazine ring. Explicitly, the strong band at 1109 cm^{-1} assigned to the C=S stretching vibration is absent in the polymers due to the absence of resonance on polymerization. Similarly, bands in the range of 2899–3136 cm^{-1} are attributed to N—H stretching in triazine groups. Polymer films show bands around 1466, 1230, and 825 cm^{-1}, which are characteristic of the aromatic triazine groups. The absence of S—H bands in the range between 2500–2660 cm^{-1} and C=S band around 1109 cm^{-1} confirms the formation of disulfide bonds and thus formation of the polymer as anticipated.[20] The exactly similar ATR-IR spectra observed for blank, THPP, TCEP, and DTT films, infer that the polymer films formed in the presence and absence of reducing agent are chemically identical (Figure S4, Supporting Information). The elemental composition of the polymer films was further validated by X-ray photoelectron spectroscopy (XPS) measurement. The S 2p photoelectrons lines can be clearly identified for all the samples including TTCA monomers and the polymer samples, both in powder form and thin films, as shown in Figure 2D. The S 2p doublet of the TTCA monomers with S $2p_{3/2}$ at a binding energy of 162.7 eV is assigned to the C=S species. For all the polymer samples S $2p_{3/2}$ shifts clearly to a higher binding energy of 164.8 eV and is attributed to the C—S—S—C species confirming the formation of disulfide polymers on oxidative polymerization of TTCA monomers.[23] C 1s spectrum (Figure 2E) shows
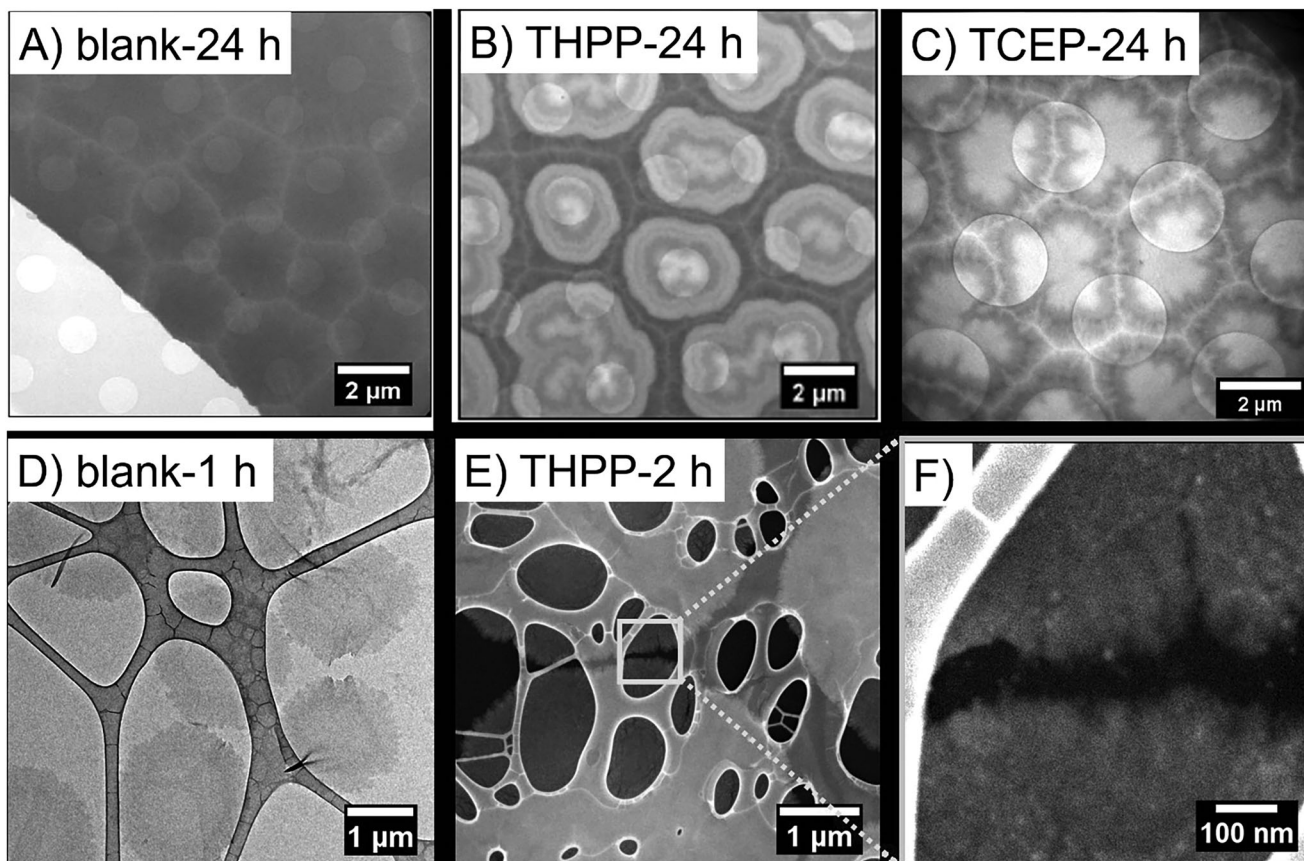
two main contributions, the most intensive one at 288.1 eV assigned to N=C—N[24] and a second one at 285.0 stemming from the usual observed surface contamination. This also explains the presence of two oxidized carbon species in a low amount and the corresponding oxygen species (O 1s not relevant here). N 1s spectrum (Figure 2F) shows a peak at 399.7 eV (C=N—C) in the ratio of 1:1 with C 1s at 288.1 eV, confirms the presence of triazene rings in the films. In addition, no P 2p peaks were detected in the THPP and TCEP films (Figure S5, Supporting Information). Considering the C=S to S—S peak ratio of 0.02 for the THPP, TCEP, and DTT films, establishing a correlation with corresponding reducing ability is not obvious. Nevertheless, the two times higher ratio (0.04) observed in the case of blank samples, this attribute is most probably in agreement to the self-correcting trait induced by the reducing agents.

To investigate the textural features of the polymer films, atomic force microscopy (AFM) was used in Peak Force tapping mode to record the topography (Figure 1; and Figures S6–S9, Supporting Information). AFM images demonstrate and confirm the distinct surface hexagonal morphologies of polymer films formed using different reducing agents. Based on the planar and triangular TTCA monomers, as anticipated, a hexagonal base structure is observed. In comparison to the blank samples, periodically well-organized and more pronounced regular hexagonal motifs are observed in the case of THPP, distorted hexagons for the TCEP, and homogenous thinner hexagons in the case of DTT. These observations were further validated by the transmission electron microscope (TEM) images (**Figure 3**A–C), showing a distorted hexagonal base structure in blank film. Similar base structure merged with distorted hexagonal crystallites was observed in the case of THPP and TCEP films. Furthermore, we collected the (S)TEM images of the blank (6 nm) and THPP (34 nm) films after 1 and 2 h of reaction time, respectively. In both cases, we observed separated islands of 2 and 4 μm in diameter, respectively, within the film. From the (S)TEM image (Figure 3D,F) of the THPP sample, we deduced that islands with their own boundaries are close enough within the range of less than 100 nm and farther apart on microscale. We presume that the disulfide films follow the "birth-and-spread mechanism,"[25] where the initial crystallites emerge by the oxidative polymerization of thiols. Crystallite growth could then proceed via incorporation of planar rigid monomers arranged on the surface under the influence of confined growth at interface.[19b] In parallel to the oxidative coupling of thiols, reducing agents induce disulfide bond dissociation and regulate the crystal growth process with corresponding reducing ability resulting in patterned films with distorted hexagonal crystallites. Apparent differences observed in the film thickness (film growth) and surface textures under similar reaction conditions with different reducing agents are plausibly attributed to different reaction kinetics.

To further investigate, imaging ellipsometry was applied to characterize the thickness and morphology of the polymer films. The simultaneously obtained optical properties are discussed further below. For the studies, all films were grown for a standard reaction time of 24 h and transferred to commercially available silicon wafer substrates. Differently colored regions can be observed by the naked eye in all samples owing to variations in the film thickness (Figure 2G–K, insets). A gradual increase in the film thickness from the peripheries to the center of the

Figure 2. Characterization of $C_3N_3S_3$ triazine polymer thin-films by. A) Raman, B) ATR-IR. C) TEM cross-section showing a thin film lamellar structure (scale bar represents 1 µm for top image and 50 nm for bottom image); by XPS analyses D–F) showing S 2p (161–168 eV), C 1s (282–292 eV), and N 1s (397–406 eV) regions; by imaging ellipsometry. G–K) Exemplary Imaging Ellipsometry Raw Data, Δ@505.3 nm, image width 500 µm, insets: photographic images of the film. G) Blank (gray scale scale 150°–350°). H) THPP (gray scale scale 170°–370°). I) TCEP (gray scale scale 150°–350°). J) DTT (gray scale scale 100°–300°); and K) thickness of the main phase determined at two different positions on each sample and L) WLI images showing a gradual increase in films thickness as a function of time.

**ADVANCED
SCIENCE NEWS**

www.advancedsciencenews.com

**ADVANCED
FUNCTIONAL
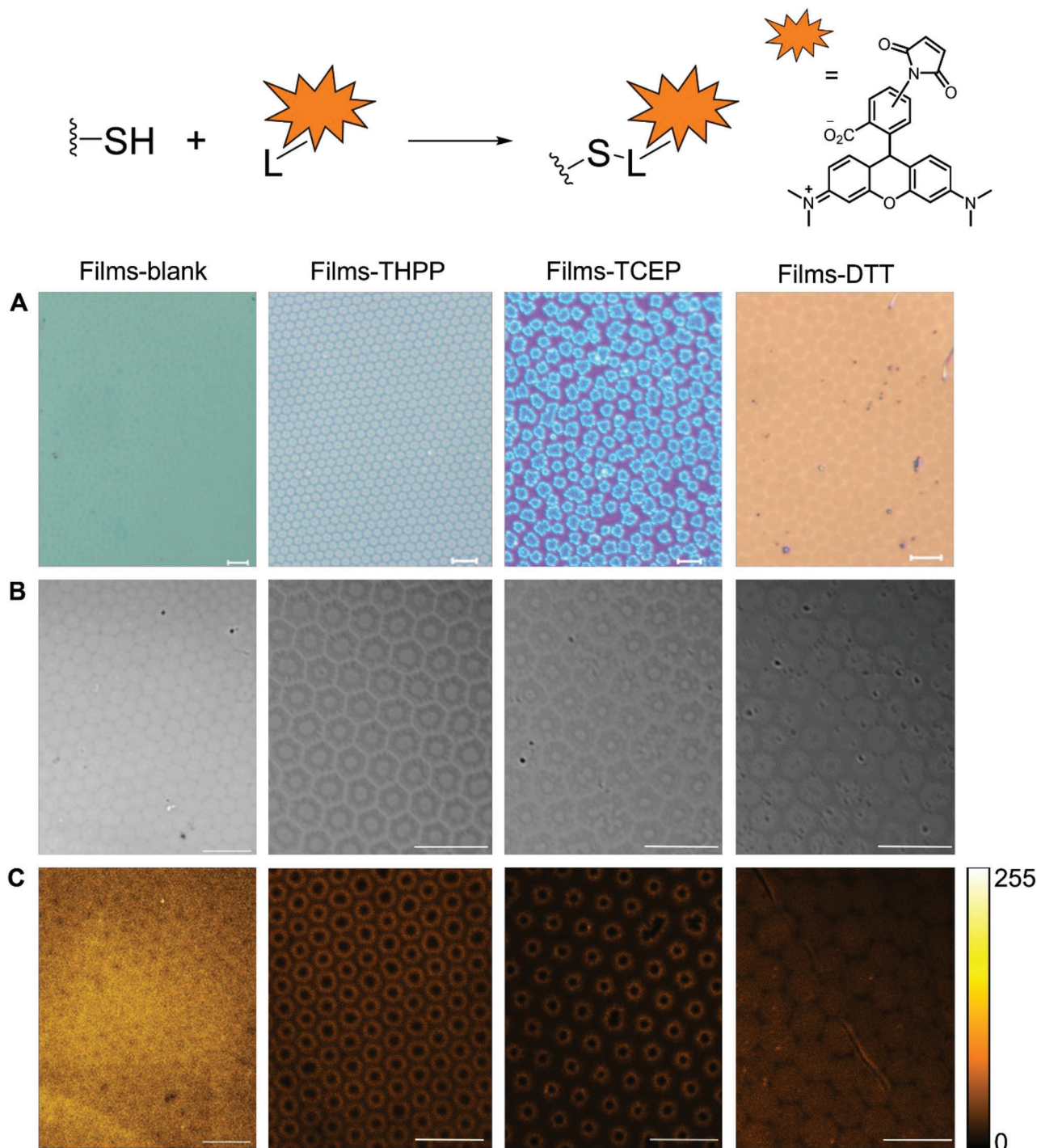MATERIALS**

www.afm-journal.de

Figure 3. TEM images of A) blank, B) THPP, and C) TCEP films collected after 24 h of reaction time. D) STEM images of blank (6 nm in thickness) and E) THPP (34 nm in thickness) films collected after 1 and 2 h, respectively, of reaction time. F) Magnified STEM image shows the edges of neighbouring crystallites in the THPP film.

film were observed in the range of 159–259, 173–292, and 169–303 nm for the blank, THPP and TCEP films, respectively. The DTT films showed streaky appearances with varying thickness in the range of 43–52 nm. The imaging ellipsometry data exhibits dotted structures in the range 50–100 μm of a ≈100 nm higher thickness than the main phase for the blank sample. On the contrast, the density of these structures is drastically reduced to almost not existent for the samples prepared in the presence of reducing agents. The reaction time plays an important role in the formation of the polymer thin-films and controlling their thickness. A gradual increase in the films thickness as a function of interfacial reaction time (2–24 h) was monitored by white light interferometry (WLI) and is shown in Figure 2L (for WLI studies, films were transferred on glass coverslips). The 2D blank film of 6 nm in thickness was observed after 1 h and gradually increases as a function of time to 162 nm in 24 h. The 2D THPP film of 35 nm in thickness was observed after 2 h, and gradually increases as a function of time to 185 nm in 24 h. By comparing the blank and THPP films, we infer that the film growth is comparatively faster in the presence of THPP reducing agent. We anticipate that this is a diffusion modulated process, permitting better monomer accessibility for the ordered film formation due to healing of defects and overgrown triazine assemblies. Furthermore, the cross-section of the interfacial 2D film exhibits precisely ordered long range lamellar structure, as evidenced by the TEM image shown in Figure 2C.

To monitor the qualitative distribution of the thiol groups on the surface of the films synthesized using different reducing agents, confocal laser scanning microscopy (CLSM) was employed. For CLSM studies, the thin film samples were placed in thiol-specific fluorescent dye solution (maleimide-TRITC (tetramethylrhodamine isothiocyanate), 4 μm in DMF) for 1 h, where samples undergo Michael-type addition reaction of thiols and maleimide, resulting in the fluorescent labeling of the thiol groups. These films were rinsed by treatment with water/DMF to remove unreacted dye precursor. Thus the relative intensity of the CLSM images correlates with pattern formation and textures on the surface (**Figure 4**). Darker regions (low fluorescence intensity) are optically distinct from thiols high coverage regions (brighter intensity). THPP and TCEP films exhibit hexagonal microstructures darker in the center and brighter at peripheries. This demonstrates that the microstructured darker regions (in the CLSM images) are lacking thiol groups, thus are comprised of denser polymers having more disulfide bonds in the center of the hexagonal motif and, comparatively, more thiol groups at the peripheries. In the case of DTT film, homogenous brightness, thus homogenous thiol distribution in the center and peripheries, is observed.

**ADVANCED
SCIENCE NEWS**

www.advancedsciencenews.com
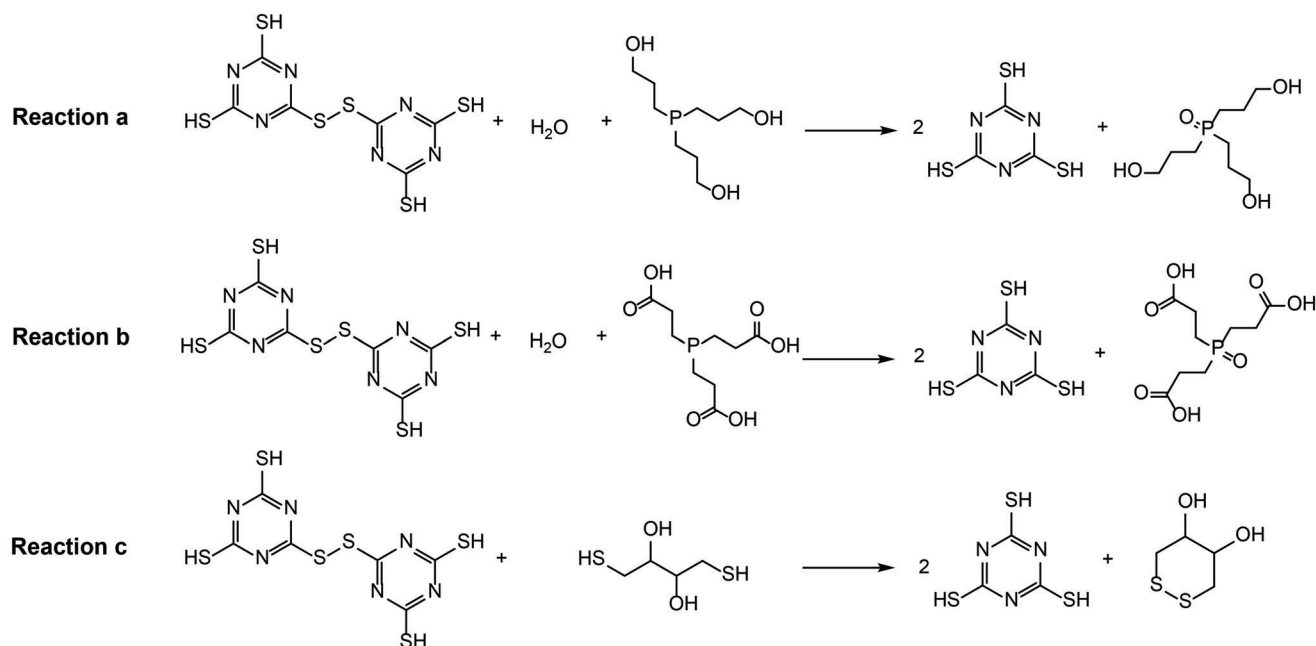
**ADVANCED
FUNCTIONAL
MATERIALS**

www.afm-journal.de

Figure 4. Microscope images of the $C_3N_3S_3$ polymer thin-films. A) digital microscope, B) CLSM images in transmission mode, and C) CLSM images in florescence red channel. CLSM samples were prepared by postfunctionalization of thiol groups with maleimide-TRITC (4 μM in DMF). In all images the scale bar is 10 μm.

2.2.1. Reaction Thermodynamics of the S—S Bond Dissociation

To rationalize experimental observations and to better understand chemical processes during oxidative disulfide based film formation in the presence of reducing agents in a one pot system, quantum-mechanical (QM) calculations and computer-aided simulations were performed. As the formation of disulfide based polymers via thiol oxidation is a well-established polymerization route, we intended to understand the influence of reducing agents on the thermodynamics of disulfide dissociation

**ADVANCED
SCIENCE NEWS**

www.advancedsciencenews.com

**ADVANCED
FUNCTIONAL
MATERIALS**

www.afm-journal.de

Figure 5. Dynamic reactions representing disulfide bond dissociation under ambient temperature and pressure in the presence of different reducing agents: a) THPP; b) TCEP; and c) DTT.

reactions. QM calculations of reactions between disulfides and three different reducing agents, i.e., THPP, TCEP, and DTT (**Figure 5**), were performed.

The structure optimization of all the reagents was performed with density functional theory (DFT) at the B3LYP[26]-D3-(BJ)[27]/def2TZVP[28] and TPSS[29]-D3-(BJ)/def2TZVP level of theory in Turbomole v.7.4. All structures were confirmed by vibrational analysis. Detailed information is provided in the Supporting Information.

Thermodynamic functions describing the S—S bond breaking in the presence of the reducing agent (**Table 1**) indicate high spontaneity of the backward reactions with the fastest bond breaking using TCEP and THPP. The Gibbs free energy of these reactions is −28.67 and −27.32 kcal mol^{-1}, using B3LYP, respectively (Table 1), with rather small impact of the implicit solvent consideration (Table S2, Supporting Information). On contrary, DTT reducing agent seems to be slightly less reactive (ΔG of −1.61

and −2.56 kcal mol^{-1} in the gas phase using B3LYP and TPSS, respectively), but still preserving the spontaneous character of the backward reaction. The solvation impact is rather small, increasing the absolute value of the energy by ≈3 kcal mol^{-1}. This agrees with the experimental observation of TCEP being a better reducing agent than DTT for the cleavage reaction of disulfide bonds.[22b,30] The combination of fast forward and backward reactions permits the dynamical nature of bond formation and breaking toward the film formation.

Due to the complexity of the process and the size of the fast growing polymer fragments, the kinetic analysis of the reactions studied was not performed. To further understand the polymer structure and the unit cell formed, the formation of various fragments was investigated. Here, both structure order (i.e., the potential to possess triazine-based rings located parallel with respect to the surface) and the energetics of the S—S bond formed (i.e., with explicit impact of cooperative effects resulting from the n-mer size) were considered. Hypothetical polymeric fragments (**Figure 6**), comprising two to eight triazine rings, were optimized in DFT.

The computed bond dissociation energies (BDE) were found to be in the range of 56–64 kcal mol^{-1} (Table S3, Supporting Information), that agree well with the experimentally reported values.[31] Data obtained shows that the six-membered units in the polymer is the most probable structural unit with the highest energy of S—S bond formed, i.e., permitting structural stability. In most of the cases of two to five triazine based polymer fragments, the formation of the distorted polymer units was detected as the most preferable one. We understand that the polymer formation process may involve not direct polymer unit formation (as depicted in Figure 6) during experiments and lots of dynamic reactions and interface processes may impact higher planarization of the polymer units (note that with the cluster approach here we
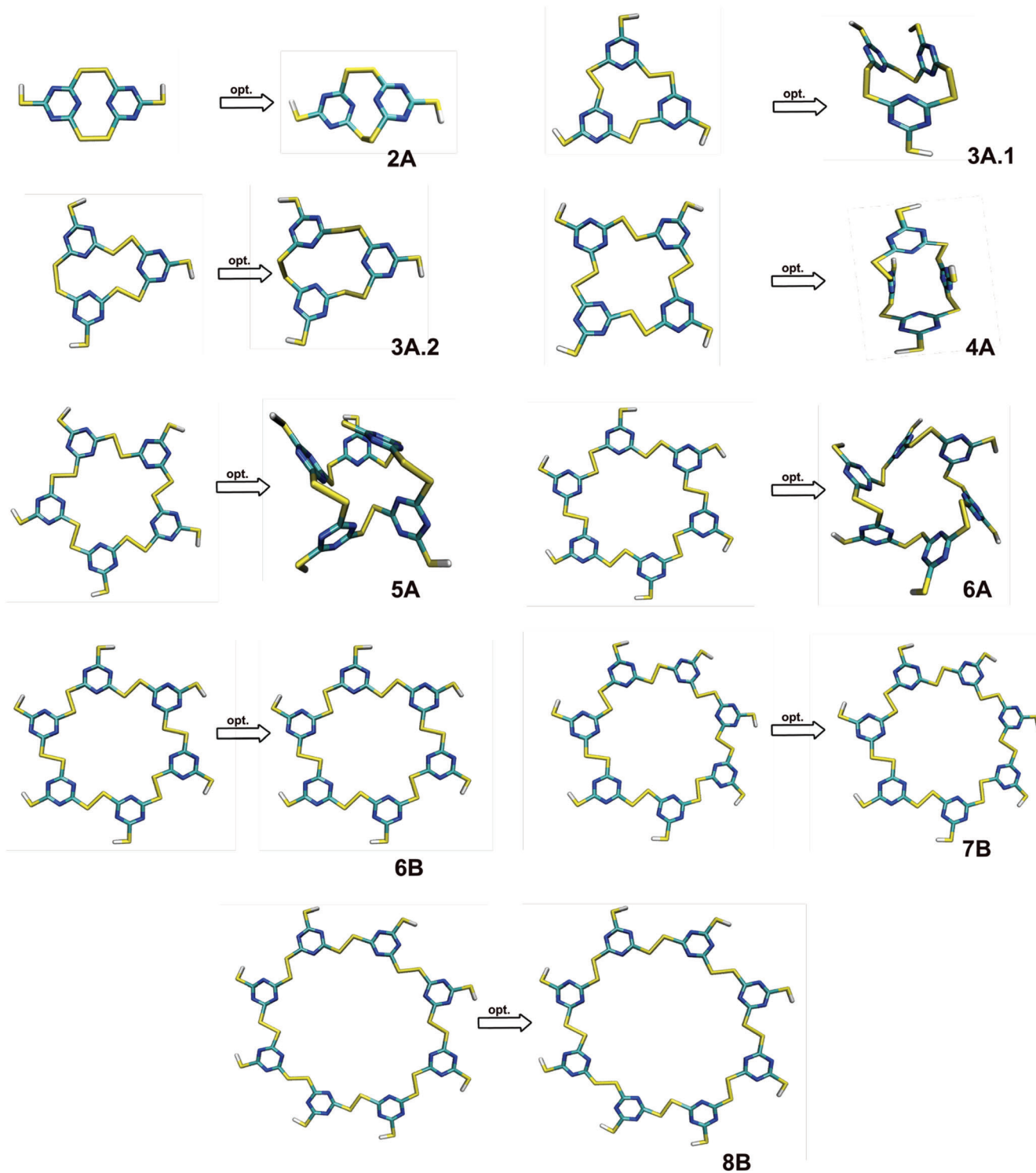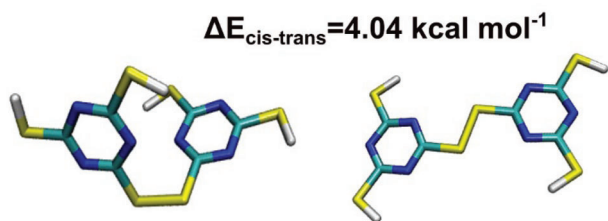
Table 1. The Gibbs free energies, enthalpy, and entropy values (in kcal mol^{-1}) of disulfide dynamic reactions (Figure 5) computed using B3LYP/def2TZVP and TPSS/def2TZVP level of theory in the gas phase under ambient temperature and pressure.

		Reaction a THPP	Reaction b TCEP	Reaction c DTT
B3LYP	ΔG	−27.32	−28.67	−1.61
	ΔH	−1.66	−1.74	−1.09
	ΔS	0.086	0.090	0.002
TPSS	ΔG	−28.61	−29.32	−2.56
	ΔH	−1.63	−1.70	−1.04
	ΔS	0.090	0.093	0.005

**ADVANCED
SCIENCE NEWS**

www.advancedsciencenews.com

**ADVANCED
FUNCTIONAL
MATERIALS**

www.afm-journal.de

Figure 6. Hypothetical polymeric units (n-unit-mers) optimized at the B3LYP-D3(BJ)/def2TZVP level of theory.

cannot properly model such effects), therefore these calculations serve only as a basic understanding. We have found the source of such deformation in the preference of *cis* S—S bond formation over the *trans* S—S (**Figure 7**) with the energy difference per one S—S bond of 4.04 kcal mol⁻¹ at 0 K. Since the gain of the

S—S bond geometry is stronger in smaller fragments, deformed units are preferable to be formed. It should be mentioned that starting from the six-membered polymer unit, higher planarization of the optimized polymer unit was found, i.e., the energy difference between two local minima is 0.845 eV (19.50 kcal mol⁻¹).

**ADVANCED
SCIENCE NEWS**

www.advancedsciencenews.com

**ADVANCED
FUNCTIONAL
MATERIALS**

www.afm-journal.de

$$\Delta E_{cis-trans} = 4.04 \text{ kcal mol}^{-1}$$

Figure 7. Representation of the cis (left) and trans (right) conformers of the formed diaryldisulfide. Rotation about the S—S axis is subject to a low barrier: Disulfides show a preference for dihedral angles C—S—S—C approaching 90°.

This shows that the interplay between the energy gain due to the geometrical preference of the polymer unit and the S—S bond formed (BDE of 64.3–61.0 kcal mol^{-1} in the distorted and planar polymer unit in the gas phase, i.e., (A) and (B) in Figure 6). Since the planar unit is more likely to result in ordered polymer, it was considered for further calculations of polymer properties.

2.3. Optical Properties

Optical properties of the polymeric films were studied by the UV–vis–NIR and imaging ellipsometry. Imaging ellipsometry studies along with refractive index and film thickness, have also provided information on structural properties like optical density, morphology, and structural anisotropy.

2.3.1. UV–Vis–NIR

The UV–vis–NIR absorption spectrum of the monomer (TTCA in THF) was first compared to the film experimental absorbance when recorded in standard 2-beam-mode. As shown in **Figure 8**, the disulfide bond formation in polymers exhibit a blueshifted absorption band at 288 nm in comparison to the TTCA monomers which show maximum absorbance at 292 nm. In addition, the polymer films' transmittance, reflectance and transflectance were recorded in an integrating sphere (details are provided in the Experimental Section). The polymer thin films exhibit a transflectance of around 99.5% in the range from 430 to 1800 nm, with around 85% transmittance and 15% reflectance. Reflection bands in the visible region seem to originate from thin-film interferences and vary with film thickness and surface roughness. Notably, the polymer films exhibit high transparency in the entire visible range and an excellent transmittance of around 85% even at 1800 nm, which expands the potential applications of disulfide polymer films in the infrared-emitting field. Very similar transflectance with an onset of absorption at 320 nm was observed in all thin film samples, and for the DTT film slightly blue shifted onset was observed. Thus, UV–vis–NIR spectra clearly indicate that the disulfide bridged triazine polymer films show a promising level of high optical transparency in the visible and NIR region.

The UV–vis absorption spectrum of the monomer (TTCA in THF), and transmittance, reflection, and transflectance spectra of the polymer films were recorded in standard 2-beam-mode

and in an integrating sphere (details are provided in the Experimental Section). As shown in Figure 8, the disulfide bond formation in polymers results in a blueshifted absorption band at 288 nm in comparison to the TTCA monomers with a maximum absorbance at 292 nm. The polymer thin films exhibit a transflectance of around 99.5% in the range from 430 to 1800 nm, with around 85% transmittance and 15% reflection. Reflection bands in the visible region seem to exist due to the surface roughness and the respective light interferences at the film surface. Notably, the polymer films exhibit high transparency in the entire visible range and an excellent transmittance of around 85% even at 1800 nm, which expands the potential applications of disulfide polymer films in the infrared-emitting field. Very similar absorptivity (1-transflectance) with the onset absorption at 320 nm was observed in all thin film samples, while in the DTT film a slightly blueshifted onset was observed. Thus, UV–vis–NIR spectra clearly indicate that the disulfide bridged triazine polymer films show a promising level of high optical transparency in the visible and NIR region.

Furthermore, degradation of the disulfide film was also confirmed by UV–vis studies. We studied the THPP-mediated depolymerization of the disulfide film by immersing the disulfide polymer film in THPP solution and the UV–vis spectrum was recorded as a function of time. To confirm depolymerization, monomer formation was detected over 24 h reaction time by UV–vis spectroscopy of the solution. An absorption band around 292 nm appeared within 5 min, on depolymerization of the polymer, gradual increase in the monomers band intensity was observed with increasing reaction time, which was attributed to the distinctive absorption band of TTCA monomer (Figure S10, Supporting Information). These results confirm that, in the presence of reducing agent, the cross-linked disulfide polymer film readily degrades and converts into smaller species. Addressing the polymer recycling challenges, the inherent bio-degradability and intriguing feature of on-demand chemical depolymerization of disulfide based materials into small-molecules make this class of materials promising for practical applications with complete materials' circularity.[32] The reversible and dynamic features of the disulfide exchange reaction intrinsically shall provide the polymeric films with self-healing properties. To investigate the self-healing characteristics, we cut the polymeric films into two pieces. Self-healing capability under controlled reaction conditions in the presence of a reducing agent works well. Details of the self-healing experiments and microscopic images are provided in the Supporting Information (Figure S11). The recycling as well as self-healing capability of the disulfide polymers via thiol-disulfide exchange reaction further highlight the importance of dynamic disulfide based functional materials.

2.3.2. Imaging Ellipsometry

The refractive index and relevant optical properties of the blank, THPP, TCEP, and DTT films (on Si-wafers) were characterized by imaging ellipsometry and the results are provided in **Figure 9**.

The optical properties of the polymeric films were determined using a uniaxial Cauchy-layer. The refractive indices show normal dispersion behavior with decreasing values as the wavelength increases. Blank, THPP, and TCEP films lie in the high

**ADVANCED
SCIENCE NEWS**

www.advancedsciencenews.com

**ADVANCED
FUNCTIONAL
MATERIALS**

www.afm-journal.de
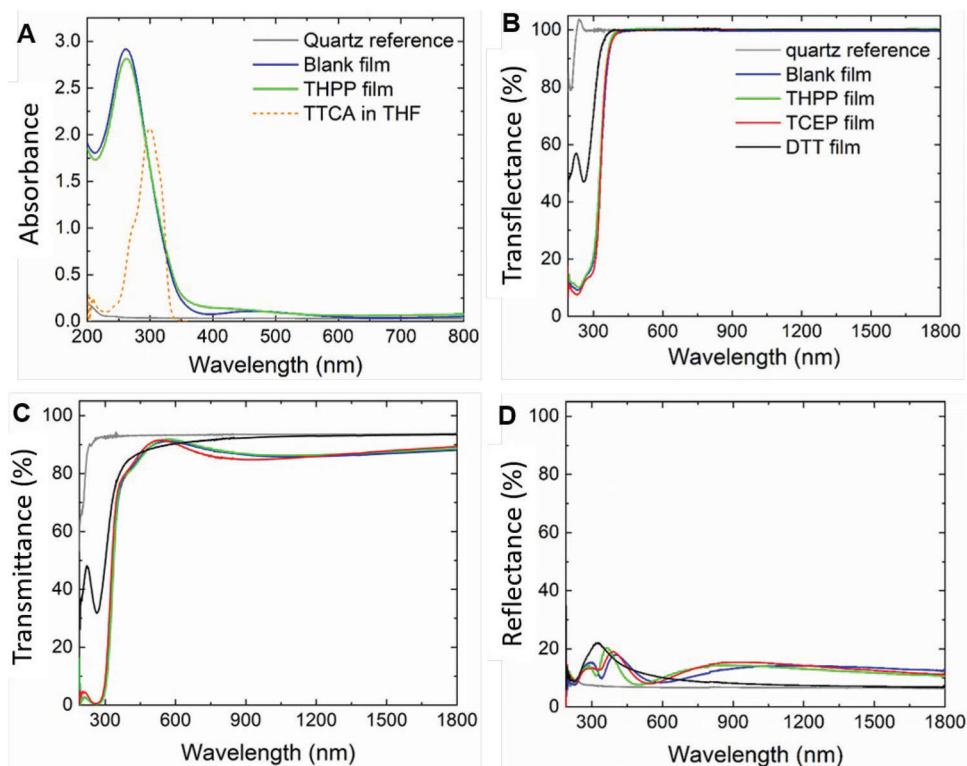
Figure 8. A) UV—vis absorption spectrum of the monomer (TTCA in THF), THPP, and blank polymer films recorded in standard 2-beam-mode. B) UV—vis—NIR transflectance. C) transmittance; and D) reflectance spectra of all the polymer films were recorded in integrating sphere. Color code in all four graphs, blank (blue), THPP (green), TCEP (red), DTT (black), and quartz reference substrate (gray).

refractive index polymer (HRIP) class with the in-plane n values of around 1.673 even at 1000 nm. The in-plane (n_o) and out-of-plane (n_e) average refractive indices and the birefringence values ($\Delta n(\lambda) = n_e(\lambda) - n_o(\lambda)$) varied only slightly over the samples with a weak trend of decreasing magnitude of birefringence from the periphery to the center of the film. The determination of the birefringence of the DTT samples was only possible with low accuracy due to parameter correlation caused by the much lower thickness. All the films exhibit linear optical anisotropy with a uniaxial negative birefringence, which is characterized by the presence of a higher refractive index along the ordinary, in-plane direction than in the extraordinary, out-of-plane direction. It is reported that the uniaxial negative birefringence is critically associated with the backbone linearity and rigidity as well as intrinsic polarizability of the polymers.[33]

In contrast to the disulfide polymer films reported in this work (with refractive indices in the range of 1.47–1.76 and with high uniaxial negative birefringence values in the range of 0.05–0.25), the analog disulfide polymer examples in the literature show significantly smaller birefringence values. For instance, for polyamide with thioether linkages $n = 1.7701$ and $\Delta n = < 0.0076$,[34] for triazine-based polyphenylene sulfides $n = 1.6902–1.7169$ and $\Delta n = 0.0015–0.0042$,[35] for poly(sulfur-*co*-dovinyl benzene) $n = 1.97$ and $\Delta n = 0.0010$,[36] for poly(2-hydroxy-1,4-phenylene sulfide) $n = 1.80$ and $\Delta n = 0.003$. The higher birefringence values observed in our systems lie well within the range of liquid-crystals polymers.[37] Our results demonstrate that the films formed are structurally precise, 2D periodic net-

works, where the disulfide bridged triazine rings impart large refractive indices along the in-plane direction with strong optical anisotropy. Notably is the appearance of extraordinary dispersion of the birefringence for the periphery of the blank and the TCEP samples and the TCEP sample overall. Here, the birefringence is almost constant over the whole wavelength range, compared to the normal dispersion with decreasing uniaxial negative birefringence with increasing wavelength. This property is of special interest for potential application of these films as optical compensators as it yields a constant retardance over a broad wavelength range.[38]

In polymers containing aromatic groups, birefringence is closely related to the anisotropy in the orientation of aromatic rings, where high anisotropy leads to high birefringence. To correlate molecular order in the polymeric films, we further performed computational studies that support the imaging ellipsometry data.

2.3.3. Refractive Index of Large Molecular 2D Network

To correlate the molecular order in 2D polymer network and the refractive index, we considered a system with perfectly ordered structure (i.e., with six-membered rings oriented parallel to the surface) and the system with slight disorder. For the perfectly ordered structure, the orientation of the normal vector of all ring structures in the system is to the surface's orientation. For the structure with disorder, a random distortion, which is described
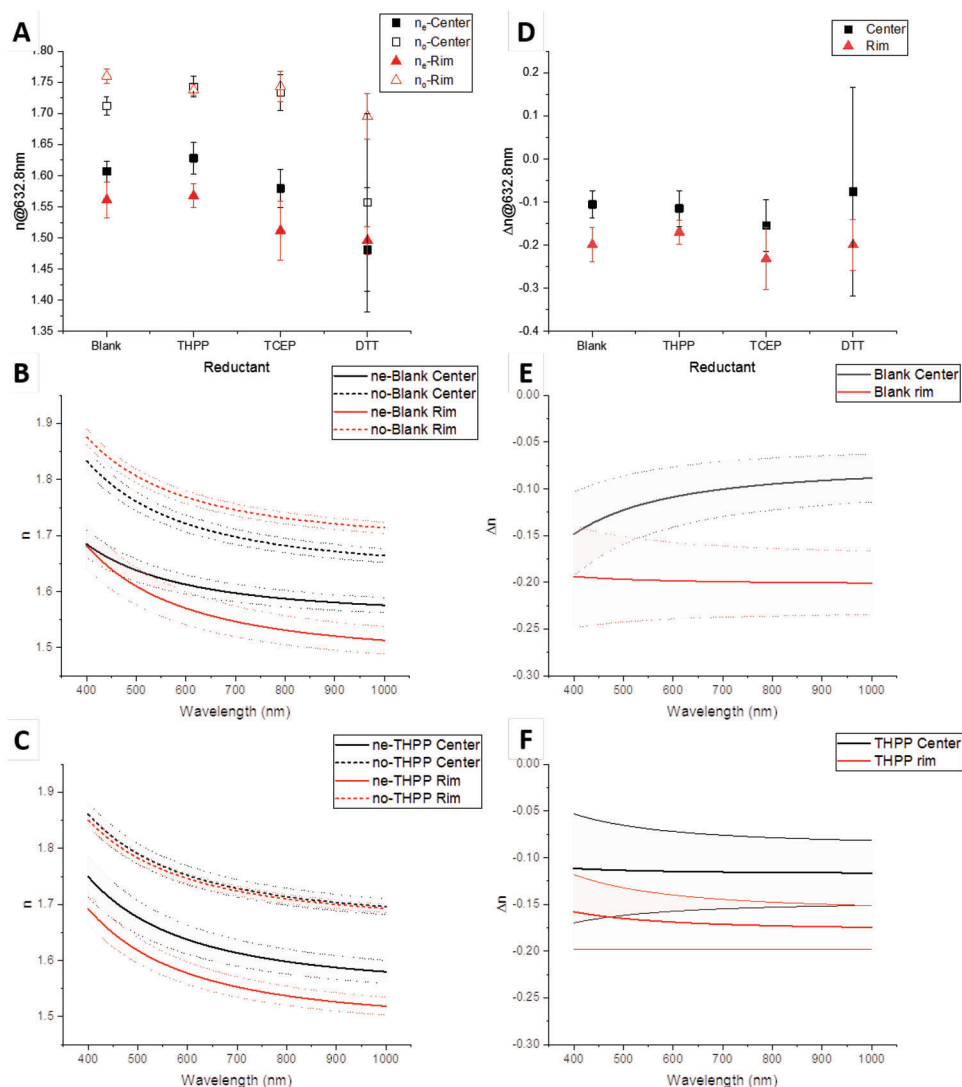
Figure 9. Optical properties of the polymer films as determined by imaging ellipsometry; ordinary and extra-ordinary refractive indices of different samples A) and the corresponding birefringence values D) each at two different locations of each sample and for a wavelength of 632.8 nm (the error bars represent the 90%-confidence values of the fit, wavelength dependent refractive index for the Blank B) and THPP sample C) and E,F) the corresponding birefringence spectra (the shaded areas represent the 90%-confidence values of the fit).

by a Gaussian distribution, was applied to the orientation of every ring structure. For the structure with slight disorder, a random distortion to orientation of every ring structure with a Gaussian distribution was introduced.
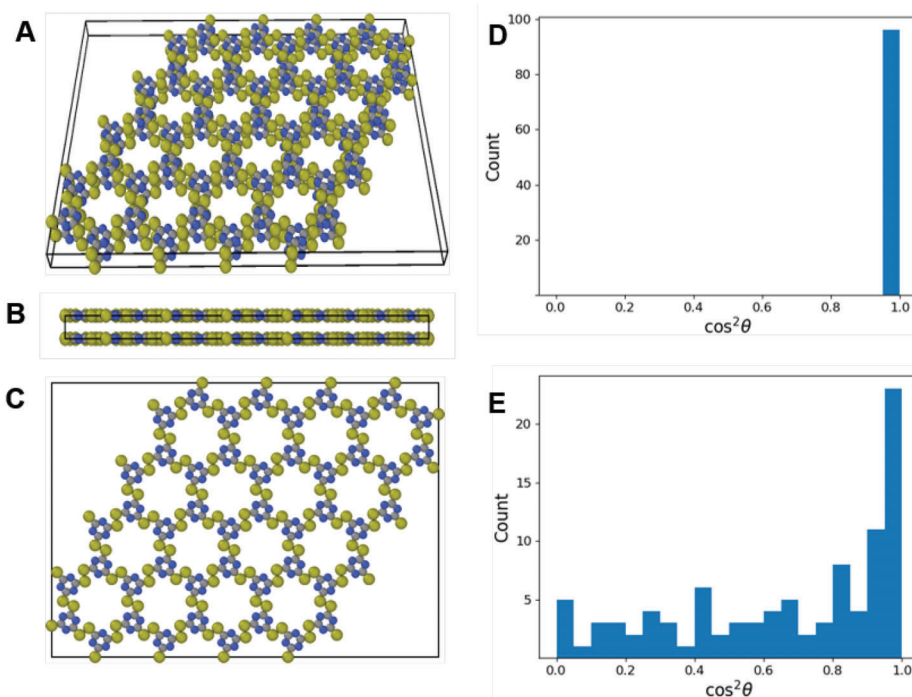
In order to quantify the molecular order, we consider an orientation parameter, which is defined as

$$\langle \cos^2 \theta_z \rangle = \frac{1}{N} \sum_i^N (n_i \cdot e_z)^2 \tag{1}$$

where n_i is the normal vector of the ring fragment i and e_z is the orientation of the normal vector in z-direction of the surface. The orientation parameter is computed from the dot product between the normal vector and the surface, corresponding to the alignment between the ring fragment and the surface. The molecu-

lar order of a polymer network structure was then analyzed by computing the average orientation parameter of all fragments in the system. When $\cos^2 \theta_z = 1$, the ring fragment is parallel to the surface. When $\cos^2 \theta_z = 0$, the ring fragment is perpendicular to it. As a result, the more ring fragments are ordered parallel to the surface, the higher is the average orientation parameter. The distributions of the orientation parameter of ring fragments of both perfectly ordered structure and structure with disorder are depicted in **Figure 10**D,E. For the ideally ordered structure, the orientation of all ring fragments equals to one. For the structure with disorder, most of the normal vectors of the fragments are not aligned parallel to the z-axis, which results in a distribution across different orientation parameters in the system.

Using Equations (S17) and (S18) (Supporting Information), the refractive index of polymer network structure with different

**ADVANCED
SCIENCE NEWS**

www.advancedsciencenews.com

**ADVANCED
FUNCTIONAL
MATERIALS**

www.afm-journal.de

Figure 10. A) The 2D planar polymer (hexamer units) structure system; B) and C) show the x-z and x-y plane of the structure, respectively. The distribution of the ring structure orientations in the polymer network with an orientation parameter, $\cos^2\theta_z$, in the system of D) perfectly ordered structure and E) structure with disorder. $\cos^2\theta_z$ accounts for the angle between the normal vector of the ring structure and the surface. The count is the number of ring structures in the polymer system with the orientation parameter.

molecular order was calculated. Both ordinary (in-plane) and extraordinary (out-of-plane) components of the refractive index are listed in **Table 2**. The refractive index in the ordinary direction is larger than in the extraordinary direction and the difference between the ordinary and extraordinary components of the refractive index $\Delta n = n_e - n_o$ of the perfectly ordered polymer network structure is larger than the one with disorder. This suggests that highly ordered polymer networks should possess a large difference between the components of the refractive index. This observation is also consistent with the studies for other materials, where similar dependence of Δn and the anisotropy of the material was reported.[39] In the next step, we calculated the orientation parameter corresponding to the refractive index values determined via spectroscopic ellipsometry for our samples using $\langle\cos^2\theta_z\rangle = 1$ for the ideally ordered system

$$\left\langle\cos^2\theta_z\right\rangle_{\text{Sample}} = \frac{\Delta n_{\text{Sample}}}{\Delta n_0} \qquad (2)$$

where Δn_0 is the birefringence for the ideally ordered system or the intrinsic birefringence of the ring fragments. The results are

Table 2. The calculated refractive index of ordered and disordered polymer network structure upon illumination at 632.8 nm.

Polymer network	n_o	n_e	Δn
Perfectly ordered	1.865	1.400	−0.464
With disorder	1.811	1.481	−0.330

displayed in **Figure 11**. The produced polymer films thus show a preferential alignment of the ring fragments parallel to the substrate, with the TCEP showing the highest orientation parameter of around 0.5 at the periphery of the sample, meaning that on
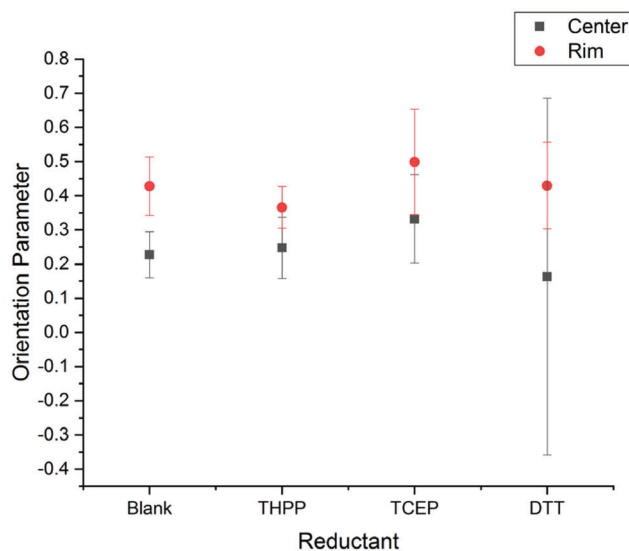
Figure 11. Orientation parameter of produced polymer films calculated from the birefringence values determined by imaging ellipsometry and the birefringence of an ideally ordered system determined by computational studies (The error bars are determined from the 90%-confident values of the ellipsometric fit).

**ADVANCED
SCIENCE NEWS**

www.advancedsciencenews.com

**ADVANCED
FUNCTIONAL
MATERIALS**

www.afm-journal.de

average 50% of the ring fragments are oriented parallel to the substrate in this location. This degree of orientation may sound low, it is still far from the random fragment orientation detected in isotropic materials.[34–36] The orientation realized with our systems lies well in the range reported for liquid-crystal polymers.[37]

3. Conclusion

In summary, we demonstrated a distinct approach for interface-confined engineering of disulfide-bridged 2D polymeric $C_3N_3S_3$ triazine thin-films by thiol-disulfide exchange process crosslinking tritopic 1,3,5-triazine-2,4,6-trithiol molecular tectons via intermolecular disulfide formation that appears also to be compatible with other function-inspired tectons bearing a flat core with predisposed multiple polymerizable thiol reactive groups at the peripheries. Taking advantage of the disulfide dynamic chemistry in combination with an interfacial polymerization strategy this approach enables the formation of covalently cross-linked 2D thin-films with controllable thickness. The $C_3N_3S_3$ triazine thin-films are dynamic in nature because of the (—S—S—) bridges, mechanically stable and can be easily transferred to other substrates or possibly into application-relevant forms for device fabrications, making this useful from materials application perspective. We prepared these polymeric thin-films on centimeter length-scale without advanced/complex instrumentation. In principle, other dimensions of polymeric thin films can be prepared by simple adjustment of the water surface area available for polymerization. To comprehend the thermodynamic properties of the disulfide dynamic processes involved in the formation of the 2D materials, QM calculations were carried out. We determined that the reduction reactions toward the S—S bond breaking are fast and spontaneous, enabling efficient dynamics of covalent bond formation in the thin-films. A set of QM calculations was also performed to get a better insight of the optimized unit cell and the early-step structure of the thin-films. The computed bond dissociation energies per S—S bond show higher preference toward *cis* conformation of the S—S bond formed (4.04 kcal mol^{-1} better than *trans*), resulting in the formation of distorted thin-films fragments (especially when 2–5 triazine molecules are forming the unit structure). However, due to the interplay of the cooperative effects of the thin-films structure geometry and S—S bond energy (of around 61 kcal mol^{-1}), the planarization of the thin-films toward highly ordered molecular structure is possible with the six triazine molecules in a hexamer unit. Experimental data revealed an outstanding optical performance of disulfide-based triazine polymer films with high transparency over the whole visible and NIR region, making them particularly intriguing for NIR imaging technologies, with large refractive indices along the in-plane direction accompanied by uniaxial negative birefringence. The refractive index of the large molecular thin-films was computed based on the Thole model via Clausius–Mossotti equation, which connects the microscopic properties and the macroscopic properties in terms of molecular polarizability and relative permittivity. It permitted us to illustrate the relation between the refractive index and its components for the ordered and disordered thin-films: highly ordered thin-films are characterized by a large difference between the ordinary and extraordinary components of the refractive index leading to uniaxial negative bire-

fringence. The comparison between the experimental and model results proof the formation of polymeric films with a high degree of preferential order. Although the film formation mechanism with more details remains to be elucidated, specific methods such as surface sensitive grazing incidence wide-angle X-ray scattering techniques could be helpful to provide more insights probing the molecular order. It may provide information about the 2D crystallites sizes, inter-molecular separation, and molecular orientation during the growth process and our future work will be focused in these directions. We believe the interfacial polymerization method, as well as the presented dynamic molecular polymeric materials could find utility in structure-dependent application possibilities, for instance in the field of optics.

4. Experimental Section

Materials: All the chemicals and solvents were used as received from the commercial sources. Chemicals include, 1,3,5-triazine-2,4,6-trithiol (TTCA, 95% from Sigma-Aldrich), Tris(hydroxypropyl)-phoshin (THPP, ≥80% from Sigma-Aldrich), DL-Dithiothreitol (DTT, ≥98% from Sigma-Aldrich), iodine (I$_2$, ≥99.8% from Sigma-Aldrich), Tris(2-carboxyethyl)phosphine hydrochloride (TCEP·HCl, Fluorochem Ltd, UK), and tetrahydrofuran for spectroscopy Uvasol (VWR Chemicals).

Stock Solutions Preparation: 1) TTCA (24.8 mg, 0.139 mmol) in a 100 mL volumetric flask was dispersed in 10 mL of THF and 80 mL of water, dissolved by sonication and the final volume was made up with distilled water. 2) THPP (2.92 mg, 0.014 mmol) in a 10 mL volumetric flask was dissolved in 1 mL of THF and 9 mL of water. 3) TCEP (4.01 mg, 0.014 mmol) in a 10 mL volumetric flask was dissolved in 1 mL of THF and 9 mL of water. 4) DTT (2.16 mg, 0.014 mmol) in a 10 mL volumetric flask was dissolved in 1 mL of THF and 9 mL of water.

Reaction Mixture Preparation: Reaction mixtures for the above mentioned four reactions A–D were prepared from the stock solution in the following ratios

Blank film: TTCA stock (20 mL), water and THF 9:1 v/v (4 mL) depicted
THPP film: TTCA stock (20 mL), THPP stock (4 mL)
TCEP film: TTCA stock (20 mL), TCEP stock (4 mL)
DTT film: TTCA stock (20 mL), DTT stock (4 mL)

Preparation of Disulfide-Triazine Thin Films: The experimental setup of the disulfide-triazine thin film formation is shown in Figure S1 (Supporting Information). The reaction mixture of the above mentioned four reactions were prepared in separate beakers (Ø 6 cm) and these four beakers were placed in a desiccator (170 × 250 mm^2). 100 mg of iodine in a 10 mL glass vial was placed in the bottom of the desiccator (the setup is shown in the Supporting Information). The reactions were left undisturbed at room temperature for 24 h. These films were rinsed by treatment with water/THF three time to removed unreacted precursor components and stored in distilled water. The polymer films stored on the water surface were transferred on demand to quartz, TEM grids or silicon wafers for spectroscopic characterizations.

Characterizations: ATR-IR spectra were collected using a Bruker Tensor 27 spectrometer equipped with a Bruker Platinum ATR accessory (diamond crystal, one reflection, angle of incidence 45°, background air). Raman spectra were collected using a Senterra II Raman microscope (Bruker Optics, Ettlingen, Germany). The excitation laser, $\lambda = 532$ nm, was operated at 6.25 mW, and the integration time for each measurement was 20 s, with four coadditions (4 × 5 s). An Olympus MPLAN 20× objective, NA 0.4 (Olympus, Tokyo, Japan), was used for visualization of the sample, focusing the excitation beam as well as for collimation of backscattered light.

Digital XPS measurements were performed using a K-Alpha+ XPS spectrometer (Thermo Fisher Scientific, East Grinstead, UK). The Thermo Avantage software was used for data acquisition and processing. All

**ADVANCED
SCIENCE NEWS**

www.advancedsciencenews.com

**ADVANCED
FUNCTIONAL
MATERIALS**

www.afm-journal.de

powders and films were analyzed using a microfocused, monochromated Al Kα X-ray source (400 µm spot size). The K-Alpha+ charge compensation system was employed during analysis, using electrons of 8 eV energy, and low-energy argon ions to prevent any localized charge build-up. The spectra were fitted with one or more Voigt profiles (BE uncertainty: ± 0.2 eV) and Scofield sensitivity factors were applied for quantification.[40] All spectra were referenced to the C 1s peak (C—C, C—H) at 285.0 eV binding energy controlled by means of the well-known photoelectron peaks of metallic Cu, Ag, and Au, respectively. Microscope images were collected using a Keyence VHX 900F (Osaka, Japan) microscope, equipped with two zoom lenses and magnification range between 20 and 2000. The image sensor is composed of micro lenses, color filters, and photodiodes. Image sensors gather light intensity information, in order to create a color image, a RGB (red, green, blue) color filter is placed in front of the photodiodes. The absorbance was determined from direct optical transmittance of thin film samples on quartz substrates and monomers in THF solution recorded in double-beam mode with a UV–vis–NIR spectrophotometer (Agilent Cary 5000). The monomers absorbance was measured with a THF-filled cuvette placed in the reference beam. The reflectance, transmittance, and transflectance spectra of the thin films on quartz substrates were measured employing an integrating sphere (Agilent External DRA-1800 with Small Spot kit) and under normal light incidence for transmittance (sample in front of sphere), close-to-normal (8°) incidence for reflectance (sample at the back of the sphere) and at 15° incidence for transflectance (center-mounted sample within the integrating sphere). The atomic force microscopy (AFM) measurements were performed on a Dimension Icon Atomic Force Microscope (Bruker, USA) operated in Peak Force Quantitative Nanoscale Mechanical mode. A Scanasyst-Fluid probe (Bruker, USA) was used, with nominal values of $k = 0.7$ N m^{-1}, radius = 20 nm, and = 150 kHz. The probe oscillated along the vertical axis in off-resonance at 2 kHz. The image resolution was 256×256 pixels, and the analysis of the AFM data was performed by Gwyddion software. For the TEM images, disulfide thin film samples were transferred from the water surface onto TEM grids with an ultrathin carbon support film or placed on Quantifoil films with support less round holes. (S)TEM data were acquired with an image-side aberration corrected FEI Titan with a CEOS corrector, operated at a primary energy of 300 keV (TEM) or a FEI Osiris microscope, operated at 200 keV (STEM). The spherical aberration for TEM was tuned to be 2 µm, and images were acquired using a 4 k CMOS camera (TVIPS XF416). Data were analyzed with GMS 3 and ImageJ. Imaging ellipsometry was performed using a multi-wavelength imaging null-ellipsometer (nanofilm ep4, Accurion GmbH, Göttingen, Germany). Measurements were taken at an angle of incidence of 50° in the wavelength range of 400–800 nm. To evaluate the experimental data, an optical box model was used. Silicon substrates were fitted with database values for Si and SiO$_x$. The optical properties of the polymer were fitted by a uniaxial Cauchy-layer. The optical birefringence is determined from the direction-dependent refractive indices as $\Delta n = n_{\mathrm{e}}(\lambda) - n_{\mathrm{o}}(\lambda)$ (e = extraordinary, out-of-plane direction, o = ordinary, in-plane direction). Details of the computational methods are provided in the Supporting Information.

Supporting Information

Supporting Information is available from the Wiley Online Library or from the author.

Conflict of Interest

The authors declare no conflict of interest.

Data Availability Statement

The data that support the findings of this study are available from the corresponding author upon reasonable request.

[1] a) K. Geng, T. He, R. Liu, S. Dalapati, K. T. Tan, Z. Li, S. Tao, Y. Gong, Q. Jiang, D. Jiang, *Chem. Rev.* **2020**, *120*, 8814; b) J. Sakamoto, J. van Heijst, O. Lukin, A. D. Schlüter, *Angew. Chem., Int. Ed.* **2009**, *48*, 1030.

[2] a) A. M. Evans, M. J. Strauss, A. R. Corcos, Z. Hirani, W. Ji, L. S. Hamachi, X. Aguilar-Enriquez, A. D. Chavez, B. J. Smith, W. R. Dichtel, *Chem. Rev.* **2022**, *122*, 442; b) R.-R. Liang, S.-Y. Jiang, R.-H. A, X. Zhao, *Chem. Soc. Rev.* **2020**, *49*, 3920.

[3] J. R. Hunt, C. J. Doonan, J. D. LeVangie, A. P. Côté, O. M. Yaghi, *J. Am. Chem. Soc.* **2008**, *130*, 11872.

[4] C. R. DeBlase, K. E. Silberstein, T.-T. Truong, H. D. Abruña, W. R. Dichtel, *J. Am. Chem. Soc.* **2013**, *135*, 16821.

[5] F. J. Uribe-Romo, C. J. Doonan, H. Furukawa, K. Oisaki, O. M. Yaghi, *J. Am. Chem. Soc.* **2011**, *133*, 11478.

[6] a) J. Guo, Y. Xu, S. Jin, L. Chen, T. Kaji, Y. Honsho, M. A. Addicoat, J. Kim, A. Saeki, H. Ihee, S. Seki, S. Irle, M. Hiramoto, J. Gao, D. Jiang, *Nat. Commun.* **2013**, *4*, 2736; b) P. Kuhn, M. Antonietti, A. Thomas, *Angew. Chem., Int. Ed.* **2008**, *47*, 3450.

[7] K. T. Jackson, T. E. Reich, H. M. El-Kaderi, *Chem. Commun.* **2012**, *48*, 8823.

[8] C. S. Diercks, O. M. Yaghi, *Science* **2017**, *355*, eaal1585.

[9] W. Zou, J. Dong, Y. Luo, Q. Zhao, T. Xie, *Adv. Mater.* **2017**, *29*, 1606100.

[10] a) Y. Jia, G. Delaittre, M. Tsotsalas, *Macromol. Mater. Eng.* **2022**, *307*, 2200178; b) Y. Jia, Y. Matt, Q. An, I. Wessely, H. Mutlu, P. Theato, S. Bräse, A. Llevot, M. Tsotsalas, *Polym. Chem.* **2020**, *11*, 2502; c) Q. An, I. D. Wessely, Y. Matt, Z. Hassan, S. Bräse, M. Tsotsalas, *Polym. Chem.* **2019**, *10*, 672.

[11] a) L. M. Polgar, M. van Duin, A. A. Broekhuis, F. Picchioni, *Macromolecules* **2015**, *48*, 7096; b) X. Chen, M. A. Dam, K. Ono, A. Mal, H. Shen, S. R. Nutt, K. Sheran, F. Wudl, *Science* **2002**, *295*, 1698.

[12] A. G. Orrillo, R. L. E. Furlan, *Angew. Chem., Int. Ed.* **2022**, *61*, e202201168.

[13] A. Rekondo, R. Martin, A. R. de Luzuriaga, G. Cabañero, H. J. Grande, I. Odriozola, *Mater. Horiz.* **2014**, *1*, 237.

**ADVANCED
SCIENCE NEWS**

www.advancedsciencenews.com

**ADVANCED
FUNCTIONAL
MATERIALS**

www.afm-journal.de

[14] R. Zhang, T. Nie, Y. Fang, H. Huang, J. Wu, *Biomacromolecules* **2022**, *23*, 1.

[15] a) C. Di Mauro, S. Malburet, A. Graillot, A. Mija, *ACS Appl. Bio. Mater.* **2020**, *3*, 8094; b) I. Azcune, I. Odriozola, *Eur. Polym. J.* **2016**, *84*, 147.

[16] Y. Xu, Y. Liu, X. Hu, R. Qin, H. Su, J. Li, P. Yang, *Angew. Chem., Int. Ed.* **2020**, *59*, 2850.

[17] L. Monnereau, M. Nieger, T. Muller, S. Bräse, *Adv. Funct. Mater.* **2014**, *24*, 1054.

[18] a) Z. Ou, B. Liang, Z. Liang, F. Tan, X. Dong, L. Gong, P. Zhao, H. Wang, Y. Zou, Y. Xia, X. Chen, W. Liu, H. Qi, U. Kaiser, Z. Zheng, *J. Am. Chem. Soc.* **2022**, *144*, 3233; b) Y. Yang, Y. Chen, F. Izquierdo-Ruiz, C. Schäfer, M. Rahm, K. Börjesson, *Nat. Commun.* **2023**, *14*, 220; c) M. Matsumoto, L. Valentino, G. M. Stiehl, H. B. Balch, A. R. Corcos, F. Wang, D. C. Ralph, B. J. Mariñas, W. R. Dichtel, *Chem* **2018**, *4*, 308.

[19] a) H. Wang, Q. Wu, H. Fu, L.-Z. Wu, X. Feng, *Chem. Commun.* **2022**, *58*, 12384; b) Y. Jin, Y. Hu, M. Ortiz, S. Huang, Y. Ge, W. Zhang, *Chem. Soc. Rev.* **2020**, *49*, 4637; c) S. Clair, D. G. de Oteyza, *Chem. Rev.* **2019**, *119*, 4717.

[20] Z. Zhang, J. Long, L. Yang, W. Chen, W. Dai, X. Fu, X. Wang, *Chem. Sci.* **2011**, *2*, 1826.

[21] Y. Zhang, R. S. Glass, K. Char, J. Pyun, *Polym. Chem.* **2019**, *10*, 4078.

[22] a) S. N. Mthembu, A. Sharma, F. Albericio, B. G. de la Torre, *ChemBioChem* **2020**, *21*, 1947; b) J. McNulty, V. Krishnamoorthy, D. Amoroso, M. Moser, *Bioorg. Med. Chem. Lett.* **2015**, *25*, 4114.

[23] J. Xu, L. Luo, G. Xiao, Z. Zhang, H. Lin, X. Wang, J. Long, *ACS Catal.* **2014**, *4*, 3302.

[24] M. Li, L. Zhang, X. Fan, M. Wu, Y. Du, M. Wang, Q. Kong, L. Zhang, J. Shi, *Appl. Catal., B* **2016**, *190*, 36.

[25] H. Qi, H. Sahabudeen, B. Liang, M. Položij, M. A. Addicoat, T. E. Gorelik, M. Hambsch, M. Mundszinger, S. Park, B. V. Lotsch, S. C. B. Mannsfeld, Z. Zheng, R. Dong, T. Heine, X. Feng, U. Kaiser, *Sci. Adv.* **2020**, *6*, eabb5976.

[26] A. D. Becke, *J. Chem. Phys.* **1993**, *98*, 5648.

[27] S. Grimme, S. Ehrlich, L. Goerigk, *J. Comput. Chem.* **2011**, *32*, 1456.

[28] A. Schäfer, H. Horn, R. Ahlrichs, *J. Chem. Phys.* **1992**, *97*, 2571.

[29] Y. Kanai, X. Wang, A. Selloni, R. Car, *J. Chem. Phys.* **2006**, *125*, 234104.

[30] E. B. Getz, M. Xiao, T. Chakrabarty, R. Cooke, P. R. Selvin, *Anal. Biochem.* **1999**, *273*, 73.

[31] O. Dmitrenko, C. Thorpe, R. D. Bach, *J. Org. Chem.* **2007**, *72*, 8298.

[32] a) Q. Zhang, D.-H. Qu, B. L. Feringa, H. Tian, *J. Am. Chem. Soc.* **2022**, *144*, 2022; b) Q. Zhang, Y. Deng, C.-Y. Shi, B. L. Feringa, H. Tian, D.-H. Qu, *Matter* **2021**, *4*, 1352.

[33] F. Li, E. P. Savitski, J.-C. Chen, Y. Yoon, F. W. Harris, S. Z. D. Cheng, *Photonic and Optoelectronic Polymers*, Vol. *672*, American Chemical Society, Washington DC **1997**, Ch. 1, p. 2.

[34] A. Javadi, Z. Najjar, S. Bahadori, V. Vatanpour, A. Malek, E. Abouzari-Lotf, A. Shockravi, *RSC Adv.* **2015**, *5*, 91670.

[35] M.-C. Fu, M. Ueda, S. Ando, T. Higashihara, *ACS Omega* **2020**, *5*, 5134.

[36] W. Jang, K. Choi, J. S. Choi, D. H. Kim, K. Char, J. Lim, S. G. Im, *ACS Appl. Mater. Interfaces* **2021**, *13*, 61629.

[37] Y. Arakawa, H. Kuwahara, M. Tokita, G.-i. Konishi, H. Tsuji, *Mol. Cryst. Liq. Cryst.* **2018**, *662*, 197.

[38] Y. Saitoh, in *Handbook of Visual Display Technology* (Eds: J. Chen, W. Cranton, M. Fihn), Springer International Publishing, Cham **2016**, p. 2277, https://doi.org/10.1007/978-3-319-14346-0_209.

[39] a) U. Goeschel, H. Lee, D. Y. Yoon, R. L. Siemens, B. A. Smith, W. Volksen, *Colloid. Polym. Sci.* **1994**, *272*, 1388; b) Y. Terui, S. Ando, *J. Polym. Sci., Part B: Polym. Phys.* **2004**, *42*, 2354; c) C. Degitz, M. Konrad, S. Kaiser, W. Wenzel, *Org. Electron.* **2022**, *102*, 106439.

[40] J. H. Scofield, *J. Electron. Spectrosc. Relat. Phenom.* **1976**, *8*, 129.